

MAPPING AGRICULTURAL WATER PRODUCTIVITY FOR CENTER PIVOT IRRIGATION SYSTEMS BASED ON SATELLITE DATA

Mahmoud A. Badr^{1&*}, Mohammed A. El-Shirbeny², Mohammed Y. El-Ansary³ and Montaser A. Awad⁴

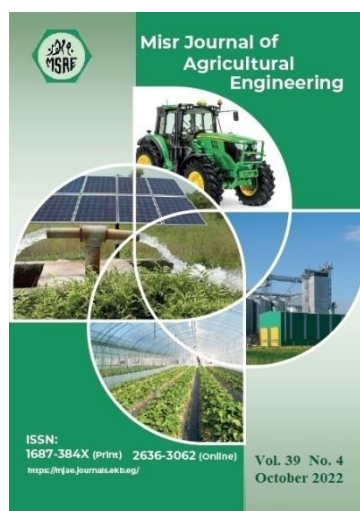
¹ PhD Stud., Ag. Eng. Dept., Fac. of Ag., Benha U., Egypt.

² Assoc. Prof. of Ag. Eng., NARSS, Egypt.

³ Prof. of Ag. Eng., Ag. Eng. Dept., Fac. of Ag., Benha U., Egypt.

⁴ Assoc. Prof. of Ag. Eng., Ag. Eng. Dept., Fac. of Ag., Benha U., Egypt.

* E-mail: ma.badr3@yahoo.com



© Misr J. Ag. Eng. (MJAE)

Keywords:

Evapotranspiration; Biomass;
Light Use Efficiency (LUE);
Remote sensing; Pivot
Irrigation System.

ABSTRACT

Developing and launching many remote sensing satellites with varying spatial-temporal accuracy, have provided various types of data at spatial, spectral, radiometric, and temporal scales, therefore, mapping agricultural ecosystems' physical and ecological characteristics with high accuracy became available by integrating remote sensing models with meteorological data. The primary goal of this research is to determine the agricultural water productivity under center pivot irrigation systems based on satellite data analysis. Landsat 8 images, agrometeorological stations, and the use of the light Use Efficiency model of Monteith (LUE) and SSEB (Simplified Surface Energy Balance) models were used to calculate the amount of crop production biomass (BIO) and The amount of water consumed, represented by the actual evapotranspiration (ET), respectively, and then, based on ET, the water productivity was determined. ($WP = BIO/ET$). The average ET, BIO, and WP values in 2021 summer season crops, ranged from 3.01 ± 1.73 to 4.1 ± 2.35 $mm\ day^{-1}$; 96.4 ± 55.4 to 191.6 ± 110.2 $kg\ ha^{-1}\ day^{-1}$; and 1.64 ± 0.94 to 2.43 ± 1.4 $kg\ m^{-3}$, respectively. The average water productivity values for the crops cultivated in the research region ranged from 1.1 to 1.4 $Kg\ m^{-3}$ for watermelon, 1.1 to 1.6 $Kg\ m^{-3}$ for peanut, 3 to 3.3 $Kg\ m^{-3}$ for Alfalfa, and 1.3 to 2.1 $Kg\ m^{-3}$ for maize. These findings demonstrate that water productivity estimates derived from remote sensing data may be utilized as an indication for increasing water rationalization via improved land and water management methods.

1. INTRODUCTION

The rising population densities throughout the globe, along with the dramatic shift in the climate, will almost certainly impact the availability of food and water for various years to come, according to experts (Fonseca et al., 2022). Egypt has another problem, besides the ones already stated, which is the construction of dams on the Nile, which

is the country's primary supply of fresh water. Because of this, it is critical to make the most of the available water unit to the greatest extent workable.

A change in land use and land cover patterns can occur as a result of a variety of different human activities. Crop production systems are reliant on a variety of inputs, including water, soil, and climate. Human activities can create major changes in evaporation, water balance, and the volume and quality of surface and groundwater if they are not effectively managed **(FAO, 2019)**.

Weather is a major predictor of agricultural production in all places with different environmental conditions, and irrigated agriculture relies on data on agriculture and meteorology to perform effective management, as well as provide the required volume of water to compensate for hydric deficits in agricultural crops. **(Beillouin et al., 2020)**.

Irrigation in Egypt depends on surface water, as it is the main source to meet the water needs of crops, represented by the Nile River. As a result, research on the most efficient use of water for optimum crop production must be undertaken, as well as the creation and deployment of technologies for water usage analysis and planning. **(Abuzai, and Jahin, 2021)**.

The center pivot irrigation systems, next to the drip irrigation system, are the modern trends that are directed to reduce water use, but with the increase of installed equipment, an increase in water consumption can occur. Therefore, work must be done on how to provide water to the appropriate spot in the field in the right quantity and at the right time, as well as to gather information to aid in the water management **(Gabr and Fattouh, 2021)**.

Remote sensing techniques have now become one of the most important tools used for environmental analysis, and its applications in agriculture, along with data related to meteorological information, enable us to map the biophysical properties of all the elements on the earth's surface can be monitored by these techniques with a great degree of precision **(Wang et al., 2018)**.

The numerous uses of these models provide a wealth of valuable information about surface energy balance flow estimates. Especially for irrigated crops, as well as the analysis of water consumption for agricultural ecosystems **(Sadras et al., 2015)**.

Estimating water productivity from satellite data on a wide scale is a very crucial support tool for agricultural policy decision-makers and planners in their decisions regarding the use of natural resources **(Jiang et al., 2015)**. Providing water for plants leads to an increase in production biomass (BIO) and evapotranspiration (ET) **(Antônio et al. 2012 and Teixeira et al. 2013)**. These are agro-environmental indicators to assess water productivity in agricultural systems.

The process of photosynthesis in plants to create (BIO) depends on Photosynthetically Active Radiation (PAR). In this process, chlorophyll, which is responsible for the process of photosynthesis inside the cell, absorbs a portion of the short wavelength solar radiation. PAR only consumes 40 to 50 percent of the total energy of solar radiation falling on the surface of the earth. As a result, PAR is a small percentage of the solar radiation (RS) that enters the system. The visible region of the solar spectrum between 0.4 and 0.7 μm is where chlorophyll absorbs solar radiation, and this is referred to as PAR. **(Verger et al., 2017)**.

On a large scale, the quantification of BIO allows us to make comparisons between different crops and base our estimate on solar radiation. The model was created by Monteith and is

based on the notion of light-use efficiency (LUE) (**Bastiaanssen and Ali, 2003**), It is appropriate to use this method in conjunction with the parameters derived from orbital data (**Teixeira et al. 2013 and Zwart et al. 2012**). The capacity of the plant to utilize gross primary productivity per unit of absorbed photosynthetically active radiation (APAR), which is constrained by temperature and water scarcity, is referred to as LUE (**Swinnen and Van Hoolst, 2018**).

Physical water productivity (WP) is defined as the ratio of agricultural output to the amount of water consumed, while economic water productivity (WP) is defined as the value derived per unit of water consumed, and both have been used to link agricultural water use to nutrition, jobs, welfare, and the environment (**Bhattacharjee et al., 2021**).

Evapotranspiration is a factor in water productivity, and the algorithm Simplified Surface Energy Balance (SSEB) determines how much of it there is. (SSEB) permits using the Penman Monteith equation to estimate ET in conjunction with data on biophysical parameters obtained through the use of remote sensing (**Acharya and Sharma, 2021**).

Under Egyptian conditions, an algorithm with different hydrological data field conditions for agro-ecosystems with different types of cultures was developed and validated for ET-based Penman-Monteith determination and showing good results (**El-Shirbeny et al., 2018**).

With the assistance of Landsat images, metrological data, and the application of the Monteith and SSEB models to estimate the BIO and the ET, respectively, this study aims to identify the spatial-temporal agro-ecological indicators of water productivity. For effective planning and decision-making at the farmer level, for integrating data from many sources, and for creating new data, the notions of water productivity are helpful in this regard. The management of Egypt's water resources will be aided by agroecological indicators.

2. MATERIALS AND METHODS

2.1 Study Area

El-Salhia project was selected as a study area which is located in the Nile Delta's eastern part. It is bordered on one side by 30° 22' 35" and 30° 31' 19" latitudes and on the other side by 31° 55' 24" and 32° 02' 38" longitudes as shown in Fig. 1. The total area of the project is approximately 32857 Fed. The project employs two types of irrigation systems: center pivots and drip irrigation. Pivot irrigation is used for field crops and drip irrigation is used for orchards trees. There are around 130 pivots in the project. Each pivot unit irrigates around 151 acres of land. The common pivots length in the project is about 450 meter.

2.2 Climate Conditions

The climate in the study region is mostly dry and arid, according to the Köppen Climate Classification System, with precipitation accounting for less than half of total potential evapotranspiration in most years. The average Temperature on an annual basis is higher than 18 °C. The average yearly rainfall is around 20 millimeters. Winter rains reach their heaviest levels in January, with an average rainfall amounting to 6.9 mm. The maximum temperature in June is 34.6°C on average, while January is the coldest month, with an average temperature of 19.0 °C (**El-Shirbeny et al., 2021**).

2.3 Remote Sensing Data Availability

Every 16 days, the Landsat 8 and Landsat 7 ETM+ satellite takes images of the entire Earth. The Operational Land Imager (OLI) sensor and the Thermal Infrared Sensor (TIRS) sensor

on board Landsat provide two thermal bands. The Landsat 8 and Landsat 7 ETM+ satellite images used in this investigation were available from the US Geological Survey (USGS). Satellite data for model development were acquired from June to October/2021. The scenes are located at (path 176/row 039) around 10:15 AM local time with a ground resolution of 30 meters. All of the satellite images from Landsat8 and Landsat 7 ETM+ which covered the study area were used to get a larger number of images that represent the growing season. So we can increase the accuracy of the model, which will be established based on this data.

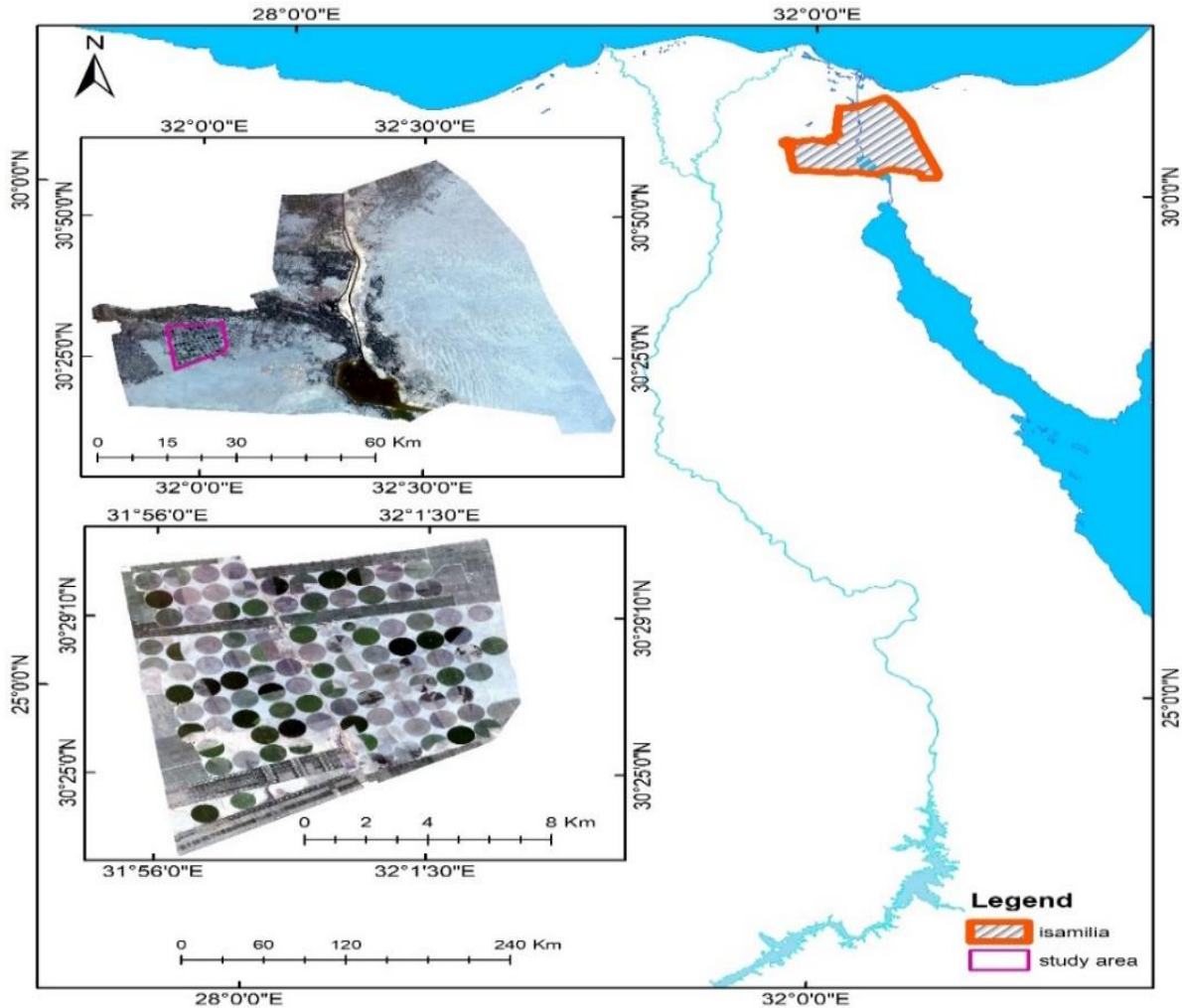


Figure 1. Location map of the study area

2.4 Remote sensed parameters

2.4.1 Land Surface Temperature (LST)

The recorded digital numbers (DN) from landsat8&7 data were converted to radiance units (Rad) using the calibration coefficients specific to each band (El-Shirbeny et al., 2014).

$$\text{Radiance} = 0.0003342 * \text{DN} + 0.10000 \quad (1)$$

The empirical equation constructed from raw data on the Normalized Difference Vegetation Index (NDVI) and thermal emissivity was used to calculate surface emissivity (Eo) using NDVI (Valor and Caselles, 1996).

$$E_o = 0.9932 + 0.0194 \ln \text{NDVI} \quad (2)$$

To compute radiant temperature (To), one must first determine the band 10 radiance (Rad10) and then use the calibration constants K1=774.89 and K2=1321.08 to get the radiant

temperature (T_o) (**El-Shirbeny et al., 2014**). The K_1 and K_2 values for landsat7 are 666.09 and 1321.08, respectively.

$$T_o = K_2 / \ln((K_1 / \text{Rad}10) + 1) \quad (3)$$

The temperature obtained as a result is the satellite radiant temperature of the observed Earth atmospheric system (in Kelvin), which is similar to but not identical to the Earth's surface (kinetic) temperature. Using satellite thermal data to provide an accurate estimate of surface temperature, it is necessary to take the effects of the atmosphere and the thermal emissivity of the surface into consideration (**Norman et al., 1995**). The Land Surface Temperature (LST) was calculated because of computing the top of atmospheric radiant temperature (T_o) and approximated surface emissivity (E_o) as follows:

$$\text{LST} = T_o / E_o \text{ (K)} \quad (4)$$

2.4.2 Normalized Difference Vegetation Index

The Normalized Difference Vegetation Index (NDVI) was calculated using two bands of remote sensing data: red and near-infrared. It is determined by the plant's reflectance in the red (R) and near-infrared (NIR) spectrum regions. This vegetation index is calculated as follows:

$$\text{NDVI} = \frac{(\text{NIR}-\text{R})}{(\text{NIR}+\text{R})} \quad (5)$$

Where: R is the reflectance in the red region and NIR is the reflectance in near infrared region of the spectrum. The scientists concluded that NDVI values are closely linked to vegetation metrics such as net primary production, leaf area index, and gross primary productivity (**Gamon et al., 1995**).

2.5 Water use mapping (actual evapotranspiration, mm)

Evapotranspiration must be estimated to determine the quantity of water utilized by crops, regardless of whether remote sensing technologies or conventional methods are used. (**Liou and Kar 2014**) found that the ET obtained from various surfaces differs with different approaches, resulting in inconsistency and ambiguity in ET estimate.

However, algorithms for surface energy balance, which are mostly based on remotely sensed data, are the best way to assess how much water crops use. The potential of remote sensing in estimating the ET (**Li et al., 2009**) is well established using Surface Energy Balance Algorithm (SEBAL) (**Bastiaanssen et al., 1999**), the modified SEBAL, and mapping ET with high resolution and internalized calibration (METRIC) (**Allen et al., 2007**). A Simplified Surface Energy Balance (SSEB) model utilising remote sensing was suggested by (**Senay and Verdin, 2003**). In this study, the SSEB technique was used to speed up the computation of water use over huge areas in a short period of time. The SSEB model is described in this manner:

$$ET_{\text{actual}} \text{ (m}^3/\text{m}^2 \text{ or m}^3/\text{pixel}) = ET_{\text{fraction}} * ET_{\text{reference}} \quad (6)$$

Remote sensing was used to calculate the ET_{actual} (expressed in m^3/ha or mm/m^2) of the water used by crops, which was calculated using the following processes: The ET_{fraction} coefficients were calculated using thermal data from Landsat8. The main premise of the SSEB model is that the latent heat flux (ET_{actual}) between the "hot" and "cool" pixels varies linearly between them. The proportion of ET's "hot" and "cool" pixels that depend on the land surface temperature (LST) was calculated (LST).

$$ET_{\text{fraction}} = (T_{\text{hot}} - T) / (T_{\text{hot}} - T_{\text{cold}}) \quad (7)$$

Where ETfraction is the fraction of ET, T is the LST of any pixel, and Thot and Tcold are the LST of "hot" and "cool" pixels picked inside the research region, respectively. Applying the Penman-Monteith formula, the ETreference was derived from weather station data (Allen et al., 1998). The final ET value for each pixel was calculated by multiplying ETfraction by ETreference, giving ETactual.

ETfraction maps were created using thermal bands from Landsat ETM+ photos obtained between June and October. For the sensor pass time, land surface temperatures were produced using the thermal bands, and locations outside the research extents were masked off. The choice of hot and cold pixels must be made with care. Despite the fact that some areas, such as concrete roadways or communities, are more likely to have greater temperatures, the hottest pixel should be chosen from dry barren farm land, where ET is virtually nil and temperature is lower. To avoid noise or the impacts of other extreme situations, numerous (5-10) pixels were chosen to calculate average values for hot (Thot) and cold (Tcold) pixels, rather than a single one. Each one's Thot and Tcold were determined.

2.6 Crop productivity mapping (kg/m²)

The Monteith's radiation model, commonly known as the Light Use Efficiency Model (LUE), estimates productivity and predicts that APAR (Wm⁻²) and maximum light use efficiency are directly proportional.

2.6.1 Photosynthetically Active Radiation – PAR

It is the portion of the sun's short-wave energy, which ranges from 0.45 to 0.5 of the solar radiation (0.3 to 3.0 μm), that helps green plants support photosynthesis (Jacovides et al., 2003). The formula for calculating PAR (Wm⁻²) is as follows:

$$PAR = aRS \quad (8)$$

In the regression equation, the constant a=0.48 reflects the amount of solar radiation that leaf chlorophyll can utilize for photosynthesis in arid and semiarid settings (Teixeira et al., 2009 b).

2.6.2 Absorbed Photosynthetically Active Radiation (APAR)

Directly from PAR, the Absorbed Photosynthetically Active Radiation (APAR) (Wm⁻²) was estimated:

$$APAR = fPAR * PAR \quad (9)$$

Based on the NDVI data (Bastiaanssen and Ali 2003; and Teixeira and Bassoi 2009 a), it may calculate the following factor, Fraction of photosynthetically active radiation (fPAR), as follows:

$$fPAR = a NDVI + b \quad (10)$$

The estimated fPAR was obtained by establishing a relationship between the NDVI and the fPAR measured on the ground represented. fPAR was determined using the AccuPAR device, which records the quantity of PAR intercepted above and below the canopy in an open field. As a result, even at the soil surface, radiation falling above the canopy can be absorbed and reflected.

2.6.3 Estimate crop production biomass (BIO) was quantified as:

The moisture effect was included in the BIO calculations using the ET_{fra} (Teixeira et al., 2018) component of the Monteith's LUE model (Monteith, 1972):

$$BIO = \Sigma (\epsilon_{\max} ET_{\text{fra}} APAR 0.864) \quad (11)$$

Where ϵ_{\max} represents the highest light use efficiency possible and 0.864 represents the unit conversion factor. For the majority crops in the study area, ϵ_{\max} of 2.4 g MJ⁻¹ was used, assuming that photosynthetically active radiation is 48% of incident solar irradiance as stated by (Gardner et al. 2017). LUE is influenced by a variety of factors, including the crop growth stage, temperature, CO₂ content in the atmosphere, and the availability of nitrogen and water.

2.7 Producing water productivity mapping (WPMs)

A division of the crop productivity map with the water usage map give us the Water Productivity Maps (WPMs). The WPMs will be as follows:

$$\text{Water Productivity Maps (kg/m}^3\text{)} = \frac{\text{Bio (kg/m}^2\text{ or kg/pixel)}}{\text{Water use (m}^3\text{ /m}^2\text{ or m}^3\text{ /pixel)}}$$

3. RESULTS AND DISCUSSION

To be used in the LUE model of BIO estimate in summer season 2021, a relation between fPAR and NDVI data has been constructed. It was determined that an empirical relationship between fPAR and NDVI could be created to calculate fPAR from remotely sensed data. Predictive functions with different mathematical forms (linear, logarithmic, power, and so on) were employed to identify the best statistical fit between the NDVI and the corresponding measured fPAR (n=45) values, with the best statistical fit being determined by the highest correlation coefficient. It was discovered via statistical analysis that the NDVI has a linear relationship with fPAR, with a coefficient of determination (R²) equal to 0.87 for both variables.

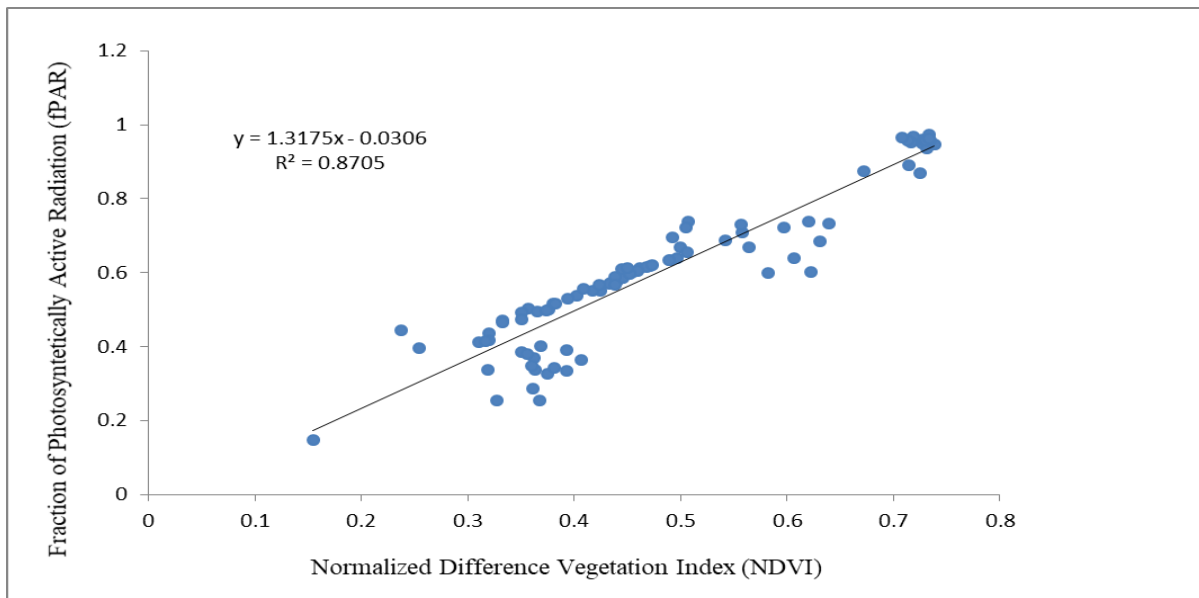


Figure 2. Relationship between NDVI and fPAR for peanuts crop during summer season 2021 and potato crop during winter season 2019.

The coefficients a and b were calculated as follows: 1.317 and -0.030, respectively. Thus, we can estimate fPAR based on NDVI data through the following linear equation:

$$\text{fPAR} = 1.317 * (\text{NDVI}) - 0.030$$

First, the monthly behavior of these meteorological parameters for the year 2021 was examined in order to better understand the monthly behavior of biophysical variables, which are predominantly influenced by solar radiation and precipitation (Figure 3). The information utilized in this study originates from the Ismailia–Ksaseen agro meteorological station in Ismailia–Ksaseen, Egypt (Latitude: 30.52 | Longitude: 31.96 | Altitude: 5 see Figure (1)).

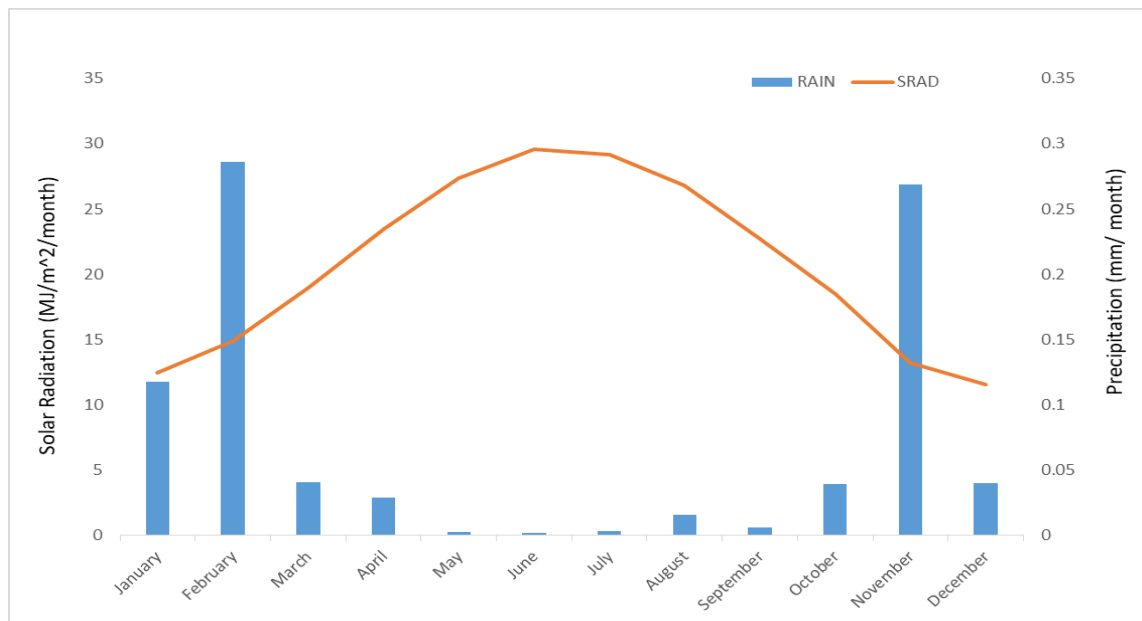


Figure 3. Recorded monthly averages of global solar radiation (RS) and total precipitation (P) for the year 2021 in Ismailia ksaseen, Egypt.

It is possible for natural vegetation as well as irrigated crops to generate enormous quantities of biomass provided adequate solar radiation and soil moisture are made accessible. The optimum conditions for natural vegetation occurred in November to March due to the amount of rain, while the best conditions for irrigated crops occurred in any month, because precipitation is not necessary for the development of plants. The total rainfall for the year 2021 was 25.18 mm. Higher levels of RS happened during the middle four months of the year. Where we notice the solar radiation begins to rise from January until it reaches its peak in July, due to the clearness of the atmosphere from the clouds and the lack of rain in the summer. Then it begins to decline again until it reaches its lowest value in the winter due to clouds and rain. In both irrigated and non-irrigated regions, the lowest solar energy availability is less beneficial for BIO.

According to (Jacovides et al., 2003), the PAR, which is around 48 percent of RS, is extraordinarily high, and when there is enough water available, this radiation is captured by crop leaves, resulting in photosynthesis taking place. Natural vegetation will generate significant quantities of BIO during the rainy season when these levels of PAR are present, however, irrigated crops will generate a significant quantity of BIO outside of this time. Following the calculation of the ET fraction as well as APAR, Equation 11 was used to calculate the BIO values on a monthly and annual basis to produce the final results. Figure 4 shows the geographic variation of the monthly BIO values for the research area for the year 2021 as depicted in the study area.

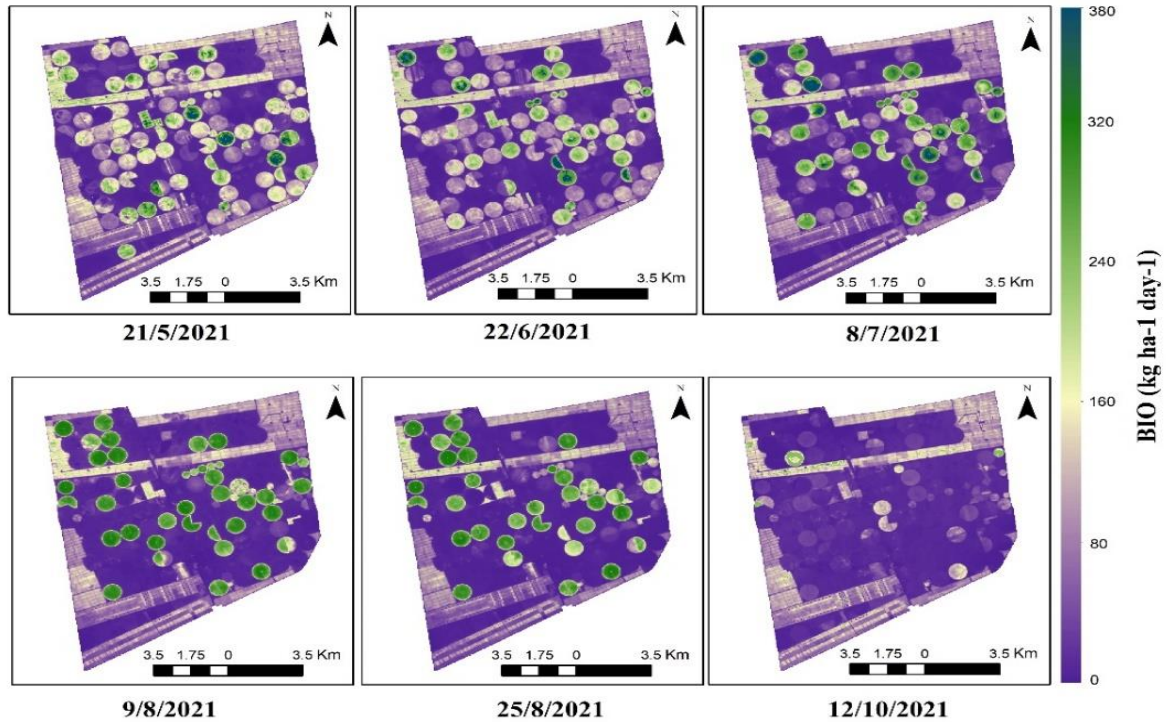


Figure 4. The spatial distribution of the daily biomass production (BIO) values during the summer of 2021 in Ismailia, El-Salhia, Egypt.

It is clear that BIO varies both spatially and temporally throughout the year. We take the summer season during 2021 to track BIO values. In the study area the end of winter season and the beginning of summer season during June. June is the month with the highest values, with some areas with BIO higher than $350 \text{ kg ha}^{-1} \text{ day}^{-1}$, with an average BIO of $300 \text{ kg ha}^{-1} \text{ day}^{-1}$ for the total area. The pivots with a high value of BIO during July and August, are the summer crops that were planted in the study area and their classification was shown in figure (5). The combined effect of increased soil moisture In addition to solar radiation leads to an increase in BIO local values. It was noted on July 8th that the largest standard deviation (STD) was observed, with a value of $80 \text{ kg ha}^{-1} \text{ day}^{-1}$, suggesting that the season had the most variability. When the crops in the region were harvested in October, the standard deviation was at its lowest, with a value of $32 \text{ kg ha}^{-1} \text{ day}^{-1}$. This was the end of the summer season and the beginning of the winter season, and the land was being prepared for the beginning of the winter season.

For the summer season of 2021, Figure 6 shows the spatial distribution of daily ET pixel values. Because there is a relationship between BIO and ET, ET values follow a similar pattern throughout the season. The maximums occurred in July and August, with an average of 7.7 mm day^{-1} . The non-cultivated pivots exhibit the lowest ET values throughout the driest months of the year, from July to October, while the irrigated pivots exhibit the greatest ET values. In general, irrigation intervals are short (daily irrigation), with a uniform water supply, lowering the heat losses to the atmosphere in irrigated pivots. Stomata close during dry natural circumstances, limiting transpiration and photosynthesis.

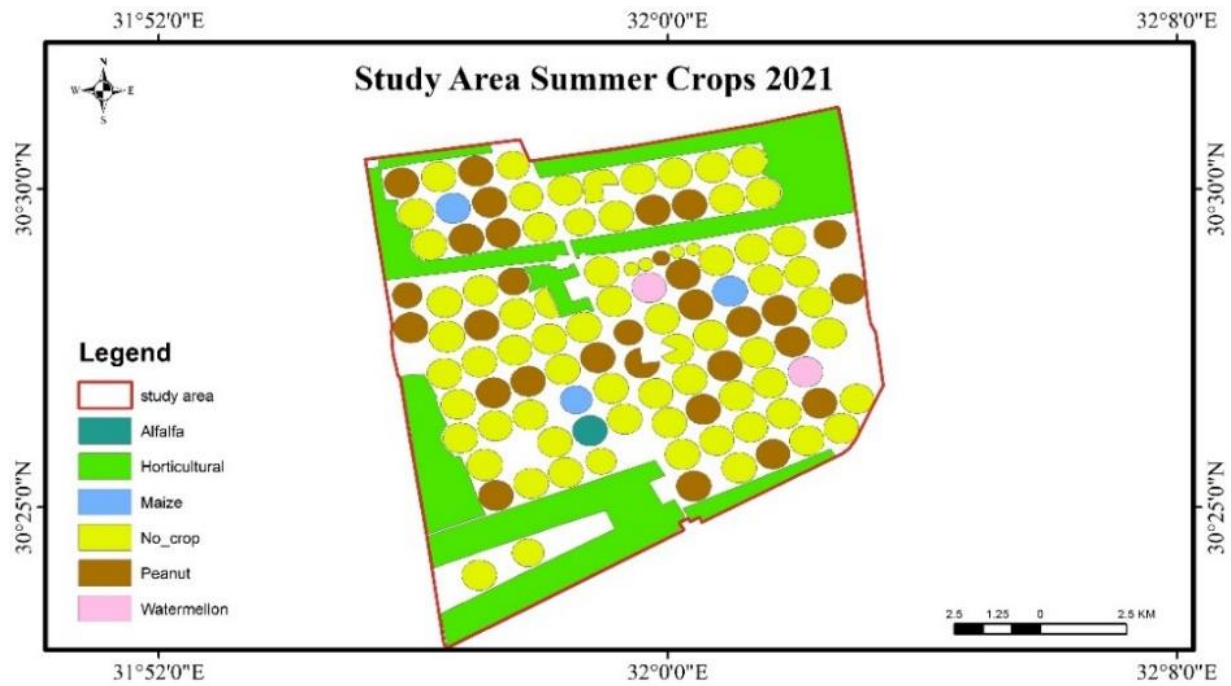


Figure 5. Map of crop types in Egypt's Ismailia_ El-Salhia region during the summer season of the year 2021.

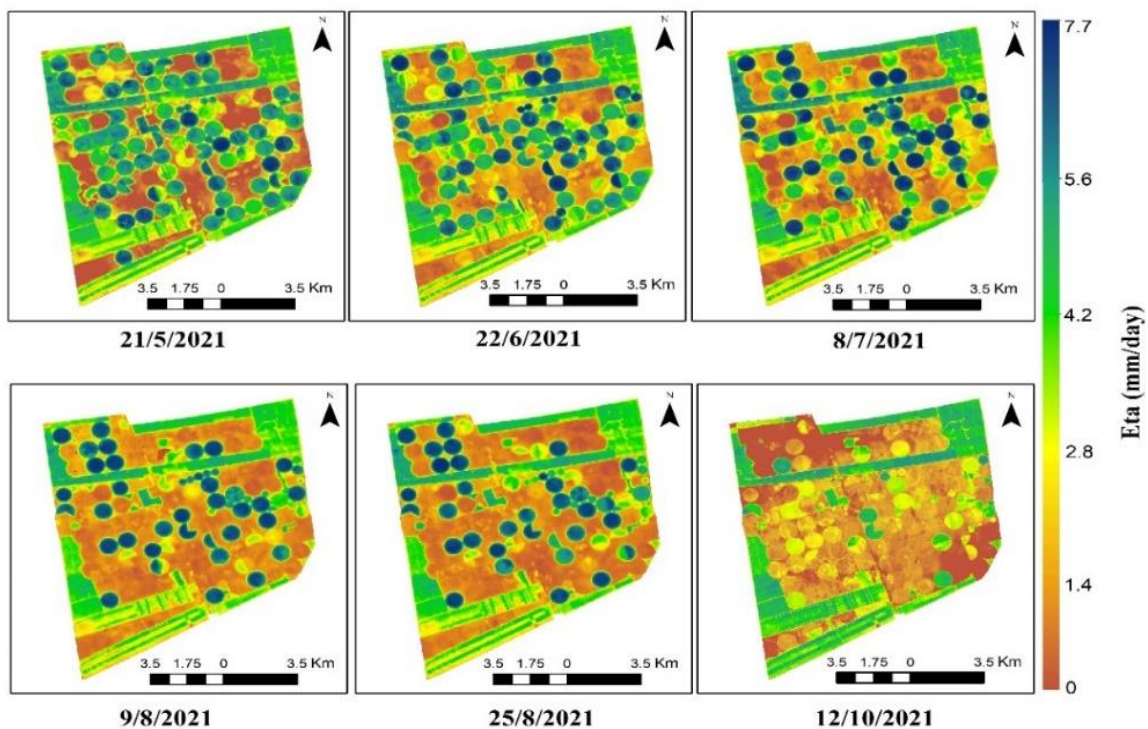


Figure 6. Actual daily evapotranspiration (ET) readings in Ismailia - El-Salhia - Egypt in summer 2021.

According to the research region, soil moisture has a significant impact on the amplitude of the ET rates (Figure 1). Pivots that have not been cultivated have pixels with values that are near 0 mm day^{-1} . The effect of variability caused by changes in cultivated pivots and non-cultivated pivots resulted in the highest (STD) value of 2.3 mm day^{-1} occurring in August as a

result of the influence of variability created by changes in cultivated pivots and non-cultivated pivots. As is the case with BIO, the month of September has the lowest standard deviation (STD) of 1.7 mm day^{-1} .

The greatest mean WP value was recorded in June, at 1.2 Kg m^{-3} (standard deviation: 1.16); the second highest mean value was recorded in July, at 1.1 Kg m^{-3} (standard deviation: 1.2). (Figure 6). Cropped pivots had the greatest WP value in June, with a maximum value of 4.80 Kg m^{-3} and a mean value of 1.2 Kg m^{-3} (standard deviation: 1.16) throughout the month.

Because it was the end of the growing season and there was little soil moisture, images taken on September 18 showed the lowest WP, with a mean value of 0.7 Kg m^{-3} (standard deviation: 0.72).

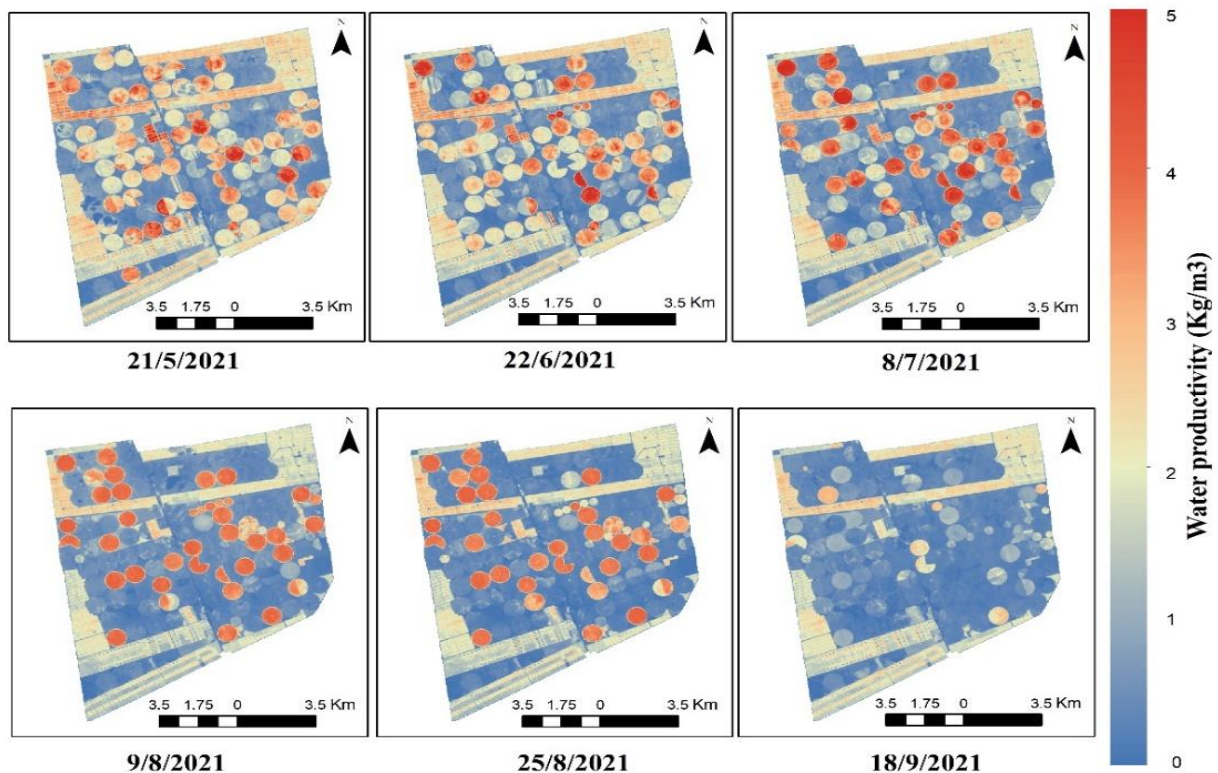


Figure 7. The Spatial distribution of the daily values of water productivity (WP) during summer season of the year 2021 in Ismailia_ El-Salhia _ Egypt.

It is feasible to calculate the crop water productivity based on ET (CWP_{ET}) by multiplying BIO by the harvest index (HI). When evaluating the WP for various forms of land use, the confirmed value for the watermelon was 1.1 to 1.4 Kg m^{-3} , for Peanut WP was 1.1 to 1.6 Kg m^{-3} , for Alfalfa WP was 3 to 3.3 Kg m^{-3} , for maize WP was 1.3 to 2.1 Kg m^{-3} . When it comes to Horticulture, the highest value was 2.8 Kg m^{-3} , the mean value was 1.9 Kg m^{-3} , and the standard deviation was 0.5 . The WP results obtained during this study were confirmed by previous studies of other researchers. WP_{ET} values of 1.1 to 1.3 kg m^{-3} for oats, 1.5 to 2.6 kg m^{-3} for sunflower, 0.5 to 1.1 kg m^{-3} for legumes, and 3.1 to 4.4 kg m^{-3} for potato were found in Inner Mongolia, which is semi-arid (Yuan et al., 2013). WP_{ET} varied from 1.9 to 2.3 kg m^{-3} for oil seed crops grown in India's semi-arid environments (Adak et al., 2013).

4. CONCLUSION

The study's major results show that satellite data and meteorological station data may be used to properly anticipate water productivity in the field. With this combination, large-scale water productivity studies across a range of Egypt's semi-arid agro-ecosystems were achievable under the Ismailia_ El Sahlia irrigation project between June and October 2021. At various times of the day, measurements of thermal, near-infrared, and visible radiation in the L8 bands were acquired from satellite data. This data was obtained by simulating the ratio of actual to reference evapotranspiration at the time of the satellite overpass, as well as by having access to daily weather data, this offered temporal data on plant reactions to changing weather and irrigation conditions as well as growth rates of the vegetation. These results suggest that water productivity estimates obtained from remote sensing data may be used as an indicator for boosting water rationalization via better land and water management approaches.

5. REFERENCES

- Abuzaid, A. S., & Jahin, H. S. (2021). Implications of irrigation water quality on shallow groundwater in the Nile Delta of Egypt: A human health risk prospective. *Environmental Technology & Innovation*, 22, 101383.
- Acharya, B., & Sharma, V. (2021). Comparison of Satellite Driven Surface Energy Balance Models in Estimating Crop Evapotranspiration in Semi-Arid to Arid Inter-Mountain Region. *Remote Sensing*, 13(9), 1822.
- Adak, T., Kumar, G., Chakravarty, N. V. K., Katiyar, R. K., Deshmukh, P. S., & Joshi, H. C. (2013). Biomass and biomass water use efficiency in oilseed crop (*Brassica juncea* L.) under semi-arid microenvironments. *biomass and bioenergy*, 51, 154-162.
- Allen, R. G., Pereira, L. S., Raes, D., & Smith, M. (1998). Crop evapotranspiration-Guidelines for computing crop water requirements-FAO Irrigation and drainage paper 56. Fao, Rome, 300(9), D05109.
- Allen, R. G., Tasumi, M., & Trezza, R. (2007). Satellite-based energy balance for mapping evapotranspiration with internalized calibration (METRIC)—Model. *Journal of irrigation and drainage engineering*, 133(4), 380-394.
- Antônio, H., Hernandez, F. B., & Lopes, H. L. (2012, October). Application of Landsat images for quantifying the energy balance under conditions of land use changes in the semi-arid region of Brazil. In *Remote Sensing for Agriculture, Ecosystems, and Hydrology XIV* (Vol. 8531, p. 85310P). International Society for Optics and Photonics.
- Bastiaanssen, W. G., & Ali, S. (2003). A new crop yield forecasting model based on satellite measurements applied across the Indus Basin, Pakistan. *Agriculture, ecosystems & environment*, 94(3), 321-340.
- Bastiaanssen, W. G., Thiruvengadachari, S., Sakthivadivel, R., & Molden, D. J. (1999). Satellite remote sensing for estimating productivities of land and water. *International Journal of Water Resources Development*, 15(1-2), 181-194.

- Beillouin, D., Schauburger, B., Bastos, A., Ciais, P., & Makowski, D. (2020). Impact of extreme weather conditions on European crop production in 2018. *Philosophical Transactions of the Royal Society B*, 375(1810), 20190510.
- Bhattacharjee, R., Choubey, A., Das, N., Ohri, A., Dwivedi, S. B., & Gaur, S. (2021). Analysis of the groundwater scenario with respect to the crop water productivity for the Betwa–Dhasan river basin, Bundelkhand using remote sensing techniques. *Journal of Earth System Science*, 130(4), 1-17.
- El-Shirbeny, M. A., Ali, A., Savin, I., Poddubskiy, A., & Dokukin, P. (2021). Agricultural water monitoring for water management under pivot irrigation system using spatial techniques. *Earth Systems and Environment*, 5(2), 341-351.
- El-Shirbeny, M. A., Mohamed, E. S., & Negm, A. (2018). Estimation of crops water consumptions using remote sensing with case studies from Egypt. Conventional water resources and agriculture in Egypt, 451-469.
- El-Shirbeny, M. A., Saleh, N. H., & Ali, A. M. (2014). Estimation of potential crop evapotranspiration using remote sensing techniques. In *Proceedings of the 10th International Conference of AARSE* (pp. 460-468).
- FAO, 2019. The State of Food Security and Nutrition in the World, Safeguarding Against Economic Slowdowns and Downturns. Food and Agriculture Organization of the United Nations,, Rome.
- Fonseca, A., Andrade, C., & Santos, J. A. (2022). Agricultural Water Security under Climate Change in the Iberian Peninsula. *Water*, 14(5), 768.
- Gabr, M. E., & Fattouh, E. M. (2021). Assessment of Irrigation Management Practices Using FAO-CROPWAT 8, Case Studies: Tina Plain and East South El-Kantara, Sinai, Egypt. *Ain Shams Engineering Journal*, 12(2), 1623-1636.
- Gamon, J. A., Field, C. B., Goulden, M. L., Griffin, K. L., Hartley, A. E., Joel, G., ... & Valentini, R. (1995). Relationships between NDVI, canopy structure, and photosynthesis in three Californian vegetation types. *Ecological Applications*, 5(1), 28-41.
- Gardner, F. P., Pearce, R. B., & Mitchell, R. L. (2017). *Physiology of crop plants*. Scientific publishers.
- Jacovides, C. P., Tymvios, F. S., Asimakopoulos, D. N., Theofilou, K. M., & Pashiardes, S. (2003). Global photosynthetically active radiation and its relationship with global solar radiation in the Eastern Mediterranean basin. *Theoretical and Applied Climatology*, 74(3), 227-233.
- Jiang, Y., Xu, X., Huang, Q., Huo, Z., Huang, G., (2015). Assessment of irrigation performance and water productivity in irrigated areas of the middle Heihe River basin using a distributed agro-hydrological model. *Agric. Water Manag.* 147, 67–81.

- Li, Z.L., Tang, R., Wan, Z., Bi, Y., Zhou, C., Tang, B., Yan, G., Zhang, X., (2009). A review of current methodologies for regional evapotranspiration estimation from remotely sensed data. *Sensors*, 9, 3801–3853.
- Liou, Y. A., & Kar, S. K. (2014). Evapotranspiration estimation with remote sensing and various surface energy balance algorithms—A review. *Energies*, 7(5), 2821-2849.
- Monteith, J. L. (1972). Solar radiation and productivity in tropical ecosystems. *Journal of applied ecology*, 9(3), 747-766.
- Norman, J. M., Divakarla, M., & Goel, N. S. (1995). Algorithms for extracting information from remote thermal-IR observations of the earth's surface. *Remote Sensing of Environment*, 51(1), 157-168.
- Sadras, V.O., Cassman, K.G., Grassini, P., Hall, A.J., Bastiaanssen, W.G.M., Laborte, A.G., Milne, A.E., Sileshi, G., Steduto, P., (2015). *Yield Gap Analysis of Field Crops, Methods and Case Studies (FAO Water Reports 41)*. FAO, Rome.
- Senay, G. B., & Verdin, J. (2003). Characterization of yield reduction in Ethiopia using a GIS-based crop water balance model. *Canadian Journal of Remote Sensing*, 29(6), 687-692.
- Swinnen, E., Van Hoolst, R., (2018). *Gio Global Land Component - Lot I “Operation of the Global Land Component”- Framework Service Contract N° 388533 (JRC). Algorithm Theoretical Basis Document, Dry Matter Productivity. Collection 300 m, Version 1. VITO, EC Copernicus Global Land, Brussels.*
- Teixeira, A. D. C., & Bassoi, L. H. (2009 a). Crop water productivity in semi-arid regions: from field to large scales. *Embrapa Semiárido-Artigo em periódico indexado (ALICE)*.
- Teixeira, A. D. C., Bastiaanssen, W. G., Ahmad, M., & Bos, M. G. (2009 b). Reviewing SEBAL input parameters for assessing evapotranspiration and water productivity for the Low-Middle Sao Francisco River basin, Brazil: Part A: Calibration and validation. *Agricultural and forest meteorology*, 149(3-4), 462-476.
- Teixeira, A.H. de C., Simão, F.R., Leivas, J.F., Gomide, R.L., Reis, J.B.R.S., Kobayashi, M.K., Oliveira, F.G., (2018). Water productivity modeling by remote sensing in the semiarid region of Minas Gerais State, Brazil. In: Arman, H., Yuksel, I. (Eds.), *Arid Environments and Sustainability*, 1st ed. InTec, London, pp. 94–108.
- Teixeira, D. C., Antônio, H., Scherer-Warren, M., Hernandez, F. B., Andrade, R. G., & Leivas, J. F. (2013). Large-scale water productivity assessments with MODIS images in a changing semi-arid environment: a Brazilian case study. *Remote Sensing*, 5(11), 5783-5804.
- Valor, E., & Caselles, V. (1996). Mapping land surface emissivity from NDVI: Application to European, African, and South American areas. *Remote sensing of Environment*, 57(3), 167-184.

- Verger, A., Baret, F., Weiss, M., (2017). Algorithm theoretical basis document: leaf area index (LAI), fraction of absorbed photosynthetically active radiation (FAPAR), fraction of green vegetation cover (FCover), collection 1km, version 2. Issue 1, 41.
- Wang, J., Ma, J., Clarke-Sather, A., & Qu, J. (2018). Estimating Changes in the Green Water Productivity of Cropping Systems in Northern Shaanxi Province in China's Loess Plateau. *Water*, 10(9), 1198.
- Yuan, M., Zhang, L., Gou, F., Su, Z., Spiertz, J. H. J., & Van Der Werf, W. (2013). Assessment of crop growth and water productivity for five C3 species in semi-arid Inner Mongolia. *Agricultural Water Management*, 122, 28-38.
- Zwart, S. J., Bastiaanssen, W. G., de Fraiture, C., & Molden, D. J. (2010). WATPRO: A remote sensing based model for mapping water productivity of wheat. *Agricultural water management*, 97(10), 1628-1636.

رسم خرائط الإنتاجية المائية لأنظمة الري المحوري بناء على بيانات الأقمار الصناعية

محمود أحمد بدر^١ محمد أحمد الشربيني^٢ محمد يوسف الأنصاري^٣ منتصر عبدالله عواد^٤

^١ طالب دكتوراه - قسم هندسة النظم الزراعية والحيوية - كلية الزراعة - جامعة بنها - مصر.

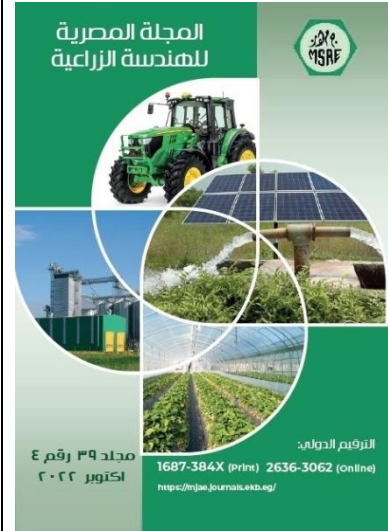
^٢ استاذ مساعد - قسم التطبيقات الزراعية - الهيئة القومية للأستشعار من البعد وعلوم الفضاء - مصر.

^٣ استاذ - قسم هندسة النظم الزراعية والحيوية - كلية الزراعة - جامعة بنها - مصر.

^٤ استاذ مساعد - قسم هندسة النظم الزراعية والحيوية - كلية الزراعة - جامعة بنها - مصر.

الملخص العربي

لقد أدى تطوير وإطلاق العديد من أقمار الاستشعار عن بعد ذات الدقة المكانية والزمانية المتفاوتة إلى توفير أنواع مختلفة من البيانات على المقاييس المكانية والطيفية والإشعاعية والزمانية، وبالتالي أصبح رسم خرائط الخصائص الفيزيائية والبيئية للنظم الإيكولوجية الزراعية متاحًا بدقة عالية من خلال دمج نماذج الاستشعار عن بعد مع بيانات الأرصاد الجوية. الهدف الأساسي من هذا البحث هو تحديد الإنتاجية المائية الزراعية في ظل أنظمة الري المحوري بناءً على تحليل البيانات المتحصل عليها من الأقمار الصناعية. تم استخدام صور القمر الصناعي (Landsat 8) ومحطات الأرصاد الجوية الزراعية واستخدام (نموذج كفاءة استخدام الضوء Monteith LUE) و (ميزان الطاقة السطحي المبسط SSEB) لحساب كمية الكتلة الحيوية لإنتاج المحاصيل (BIO) وكمية المياه المستهلكة، يمثلها التبخر الفعلي (ET)، على التوالي، وبعد ذلك، بناءً على ET، تم تحديد إنتاجية المياه. $(WP = BIO/ET)$. تراوحت قيم ET و BIO و WP في محاصيل موسم الصيف ٢٠٢١ من $3,01 \pm 1,73$ إلى $4,1 \pm 2,35$ ملم في اليوم؛ $96,4 \pm 55,4$ إلى $191,6 \pm 110,2$ كجم هكتار^{-١} يوم^{-١}؛ و $1,64 \pm 0,94$ إلى $2,43 \pm 1,4$ كجم م^{-٣}، على التوالي. تراوحت قيم متوسط إنتاجية المياه للمحاصيل المزروعة في منطقة البحث من $1,1$ إلى $1,4$ كجم م^{-٣} للبطيخ، $1,1$ إلى $1,6$ كجم م^{-٣} للذرة، 3 إلى $3,3$ كجم م^{-٣} للبرسيم، $1,3$ إلى $2,1$ كجم م^{-٣} للذرة. توضح هذه النتائج أن تقديرات الإنتاجية المائية المستمدة من بيانات الاستشعار يمكن استخدامها كمؤشر لزيادة ترشيد المياه من خلال أساليب إدارة الأراضي والمياه المحسنة.



© المجلة المصرية للهندسة الزراعية

الكلمات المفتاحية:

البخرنتح؛ الكتلة الحيوية؛ كفاءة استخدام الضوء؛ الاستشعار عن بعد؛ نظام الري المحوري.